Gravitational energy as dark energy: Average observational quantities

David L. Wiltshire

Department of Physics & Astronomy, University of Canterbury, Private Bag 4800, Christchurch 8140, New Zealand; and
International Center for Relativistic Astrophysics Network (ICRANet), P.le della Repubblica 10, Pescara 65121, Italy

Abstract. I discuss potential observational tests of a "radically conservative" solution to the problem of dark energy in cosmology, in which the apparent acceleration of the universe is understood as a consequence of gravitational energy gradients that grow when spatial curvature gradients become significant with the nonlinear growth of cosmic structure. In particular, I discuss measures equivalent to the dark energy equation of state, baryon acoustic oscillation statistic D_V, $H(z)$, the $Om(z)$ diagnostic, an average inhomogeneity diagnostic, and the time–drift of cosmological redshifts.

Keywords: dark energy, theoretical cosmology, observational cosmology
PACS: 98.80.-k 98.80.Es 95.36.+x 98.80.Jk

INTRODUCTION

I will discuss some recent results on observational tests [1] of a model cosmology, which represent a new approach to understanding the phenomenology of dark energy as a consequence of the effect of the growth of inhomogeneous structures. The basic idea, outlined in a nontechnical manner in ref. [2], is that as inhomogeneities grow one must consider not only their backreaction on average cosmic evolution, but also the variance in the geometry as it affects the calibration of clocks and rods of ideal observers. Dark energy is then effectively realised as a misidentification of gravitational energy gradients.

Although the standard Lambda Cold Dark Matter (ΛCDM) model, provides a good fit to many tests, there are tensions between some tests, and also a number of puzzles and anomalies. Furthermore, at the present epoch the observed universe is only statistically homogeneous once one samples on scales of 150–300 Mpc. Below such scales it displays a web–like structure, dominated in volume by voids. Some 40%–50% of the volume of the present epoch universe is in voids with $\delta\rho/\rho \sim -1$ on scales of $30h^{-1}$ Mpc [3], where h is the dimensionless parameter related to the Hubble constant by $H_0 = 100h\,\mathrm{km\ sec^{-1}\,Mpc^{-1}}$. Once one also accounts for numerous minivoids, and perhaps also a few larger voids, then it appears that the present epoch universe is void-dominated. Clusters of galaxies are spread in sheets that surround these voids, and thin filaments that thread them.

One particular consequence of a matter distribution that is only statistically homogeneous, rather than exactly homogeneous, is that when the Einstein equations are averaged they do not evolve as a smooth Friedmann–Lemaître–Robertson–Walker (FLRW) geometry. Instead the Friedmann equations are supplemented by additional backreaction terms [4]. Whether or not one can fully explain the expansion history of the universe as a consequence of the growth of inhomogeneities and backreaction, without a fluid–like dark energy, is the subject of ongoing debate [5].

Over the past two years I have developed a new physical interpretation of cosmological solutions within the Buchert averaging scheme [6, 7, 8]. I start by noting that in the presence of strong spatial curvature gradients, not only should the average evolution equations be replaced by equations with terms involving backreaction, but the physical interpretation of average quantities must also account for the differences between the local geometry and the average geometry. In other words, geometric variance can be just as important as geometric averaging when it comes to the physical interpretation of the expansion history of the universe.

I proceed from the fact that structure formation provides a natural division of scales in the observed universe. As observers in galaxies, we and the objects we observe in other galaxies are necessarily in bound structures, which formed from density perturbations that were greater than critical density. If we consider the evidence of the large scale structure surveys on the other hand, then the average location by volume in the present epoch universe is in a void, which is negatively curved. We can expect systematic differences in spatial curvature between the average mass environment, in bound structures, and the volume-average environment, in voids.

Spatial curvature gradients will in general give rise to gravitational energy gradients. Physically this can be understood in terms of a relative deceleration of expanding regions of different densities. Those in the denser region decelerate more and age less. Since we are dealing with weak fields the relative deceleration of the background is small. Nonetheless even if the relative deceleration is typically of order $10^{-10}\mathrm{ms}^{-2}$, cumulatively over the age of the universe it leads to significant clock rate variances [8]. I proceed from an ansatz that the variance in gravitational energy is correlated with the average spatial curvature in such a way as to implicitly solve the Sandage–de Vaucouleurs paradox that a statistically quiet, broadly isotropic, Hubble flow is observed deep below the scale of statistical homogeneity. Expanding regions of different densities are patched together so that the regionally measured expansion, in terms of the variation of the regional proper length, $\ell_r = \mathscr{V}^{1/3}$, with respect to proper time of isotropic observers (those who see an isotropic mean CMB), remains uniform. Although voids open up faster, so that their proper volume increases more quickly, on account of gravitational energy gradients the local clocks will also tick faster in a compensating manner.

Details of the fitting of local observables to average quantities for solutions to the Buchert formalism are described in detail in refs. [6, 7]. Negatively curved voids, and spatially flat expanding wall regions within which galaxy clusters are located, are combined in a Buchert average

$$f_{\rm v}(t) + f_{\rm w}(t) = 1, \tag{1}$$

where $f_{\rm w}(t) = f_{\rm wi} a_{\rm w}^{\,3}/\bar{a}^3$ is the *wall volume fraction* and $f_{\rm v}(t) = f_{\rm vi} a_{\rm v}^{\,3}/\bar{a}^3$ is the *void volume fraction*, $\mathscr{V} = \mathscr{V}_{\rm i}\bar{a}^3$ being the present horizon volume, and $f_{\rm wi}$, $f_{\rm vi}$ and $\mathscr{V}_{\rm i}$ initial values at last scattering. The time parameter, t, is the volume–average time parameter of the Buchert formalism, but does not coincide with that of local measurements in galaxies. In trying to fit a FLRW solution to the universe we attempt to match our local spatially flat wall geometry

$$\mathrm{d}s^2_{fi} = -\mathrm{d}\tau^2 + a_{\rm w}^{\,2}(\tau)\left[\mathrm{d}\eta_{\rm w}^2 + \eta_{\rm w}^2 \mathrm{d}\Omega^2\right] . \tag{2}$$

to the whole universe, when in reality the rods and clocks of ideal isotropic observers vary with gradients in spatial curvature and gravitational energy. By conformally matching radial null geodesics with those of the Buchert average solutions, the geometry (2) may be extended to cosmological scales as the dressed geometry

$$\mathrm{d}s^2 = -\mathrm{d}\tau^2 + a^2(\tau)\left[\mathrm{d}\bar{\eta}^2 + r_{\rm w}^2(\bar{\eta},\tau)\,\mathrm{d}\Omega^2\right] \tag{3}$$

where $a = \bar{\gamma}^{-1}\bar{a}$, $\bar{\gamma} = \frac{\mathrm{d}t}{\mathrm{d}\tau}$ is the relative lapse function between wall clocks and volume–average ones, $\mathrm{d}\bar{\eta} = \mathrm{d}t/\bar{a} = \mathrm{d}\tau/a$, and $r_{\rm w} = \bar{\gamma}(1-f_{\rm v})^{1/3}\, f_{\rm wi}{}^{-1/3}\eta_{\rm w}(\bar{\eta},\tau)$, where $\eta_{\rm w}$ is given by integrating $\mathrm{d}\eta_{\rm w} = f_{\rm wi}{}^{1/3}\mathrm{d}\bar{\eta}/[\bar{\gamma}(1-f_{\rm v})^{1/3}]$ along null geodesics.

In addition to the bare cosmological parameters which describe the Buchert equations, one obtains dressed parameters relative to the geometry (3). For example, the dressed matter density parameter is $\Omega_M = \bar{\gamma}^3\bar{\Omega}_M$, where $\bar{\Omega}_M = 8\pi G\bar{\rho}_{M0}\bar{a}_0^3/(3\bar{H}^2\bar{a}^3)$ is the bare matter density parameter. The dressed parameters take numerical values close to the ones inferred in standard FLRW models.

APPARENT ACCELERATION AND HUBBLE FLOW VARIANCE

The gradient in gravitational energy and cumulative differences of clock rates between wall observers and volume average ones has important physical consequences. Using the exact solution obtained in ref. [7], one finds that a volume average observer would infer an effective deceleration parameter $\bar{q} = -\ddot{\bar{a}}/(\bar{H}^2\bar{a}) = 2\,(1-f_{\rm v})^2/(2+f_{\rm v})^2$, which is always positive since there is no global acceleration. However, a wall observer infers a dressed deceleration parameter

$$q = -\frac{1}{H^2 a}\frac{\mathrm{d}^2 a}{\mathrm{d}\tau^2} = \frac{-\,(1-f_{\rm v})\,(8f_{\rm v}{}^3 + 39f_{\rm v}{}^2 - 12f_{\rm v} - 8)}{\left(4 + f_{\rm v} + 4f_{\rm v}{}^2\right)^2}\,, \tag{4}$$

where the dressed Hubble parameter is given by

$$H = a^{-1}\tfrac{\mathrm{d}}{\mathrm{d}\tau}\,a = \bar{\gamma}\bar{H} - \dot{\bar{\gamma}} = \bar{\gamma}\bar{H} - \bar{\gamma}^{-1}\tfrac{\mathrm{d}}{\mathrm{d}\tau}\,\bar{\gamma}. \tag{5}$$

At early times when $f_{\rm v} \to 0$ the dressed and bare deceleration parameter both take the Einstein–de Sitter value $q \simeq \bar{q} \simeq \frac{1}{2}$. However, unlike the bare parameter which monotonically decreases to zero, the dressed parameter becomes negative when $f_{\rm v} \simeq 0.59$ and $\bar{q} \to 0^-$ at late times. For the best-fit parameters [9] the apparent acceleration begins at a redshift $z \simeq 0.9$.

Cosmic acceleration is thus revealed as an apparent effect which arises due to the cumulative clock rate variance of wall observers relative to volume–average observers. It becomes significant only when the voids begin to dominate the universe by volume. Since the epoch of onset of apparent acceleration is directly related to the void fraction, $f_{\rm v}$, this solves one cosmic coincidence problem.

In addition to apparent cosmic acceleration, a second important apparent effect will arise if one considers scales below that of statistical homogeneity. By any one set of clocks it will appear that voids expand faster than wall regions. Thus a wall observer will see galaxies on the far side of a dominant void of diameter $30h^{-1}$ Mpc to recede at a value greater than the dressed global average H_0, while galaxies within an ideal wall will recede at a rate less than H_0. Since the uniform bare rate $\bar{H}$ would also be the local value within an ideal wall, eq. (5) gives a measure of the variance in the apparent Hubble flow. The best fit parameters [9] give a dressed Hubble constant $H_0 = 61.7^{+1.2}_{-1.1}\,\mathrm{km\ sec^{-1}\,Mpc^{-1}}$, and a bare Hubble constant $\bar{H}_0 = 48.2^{+2.0}_{-2.4}\,\mathrm{km\ sec^{-1}\,Mpc^{-1}}$. The present epoch variance is 22%, and we can expect the Hubble constant to attain local maximum values of order $72.3\,\mathrm{km\ sec^{-1}\,Mpc^{-1}}$ when measured over local voids.

Since voids dominate the universe by volume at the present epoch, any observer in a galaxy in a typical wall region will measure locally higher values of the Hubble constant, with peak values of order $72\,\mathrm{km\ sec^{-1}\,Mpc^{-1}}$ at the $30h^{-1}$ Mpc scale of the dominant voids. Over larger distances, as the line of sight intersects more walls as well as voids, a radially spherically symmetric average will give an average Hubble constant whose value decreases from the maximum at the $30h^{-1}$ Mpc scale to the dressed global average value, as the scale of homogeneity is approached at roughly the baryon acoustic oscillation (BAO) scale of $110h^{-1}$Mpc. This predicted effect could account for the Hubble bubble [10] and more detailed studies of the scale dependence of the local Hubble flow [11].

In fact, the variance of the local Hubble flow below the scale of homogeneity should correlate strongly to observed structures in a manner which has no equivalent prediction in FLRW models.

FUTURE OBSERVATIONAL TESTS

There are two types of potential cosmological tests that can be developed; those relating to scales below that of statistical homogeneity as discussed above, and those that relate to averages on our past light cone on scales much greater than the scale of statistical homogeneity. The second class of tests includes equivalents to all the standard cosmological tests of the standard model of a Newtonianly perturbed FLRW model. This second class of tests can be further divided into tests which just deal with the bulk cosmological averages (luminosity and angular diameter distances etc), and those that deal with the variance from the growth of structures (late epoch integrated Sachs–Wolfe effect, cosmic shear, redshift space distortions etc). Here I will concentrate solely on the simplest tests which are directly related to luminosity and angular diameter distance measures.

In the timescape cosmology we have an effective dressed luminosity distance

$$d_L = a_0(1+z)r_{\rm w}, \tag{6}$$

where $a_0 = \bar{\gamma}_0^{-1}\bar{a}_0$, and

$$r_{\rm w} = \bar{\gamma}(1-f_{\rm v})^{1/3}\int_t^{t_0}\frac{{\rm d}t'}{\bar{\gamma}(t')(1-f_{\rm v}(t'))^{1/3}\bar{a}(t')}\,. \tag{7}$$

We can also define an *effective angular diameter distance*, d_A, and an *effective comoving distance*, D, to a redshift z in the standard fashion

$$d_A = \frac{D}{1+z} = \frac{d_L}{(1+z)^2}\,. \tag{8}$$

A direct method of comparing the distance measures with those of homogeneous models with dark energy, is to observe that for a standard spatially flat cosmology with dark energy obeying an equation of state $P_D = w(z)\rho_D$, the quantity

$$H_0 D = \int_0^z \frac{{\rm d}z'}{\sqrt{\Omega_{M0}(1+z')^3 + \Omega_{D0}\exp\left[3\int_0^{z'}\frac{(1+w(z'')){\rm d}z''}{1+z''}\right]}}\,, \tag{9}$$

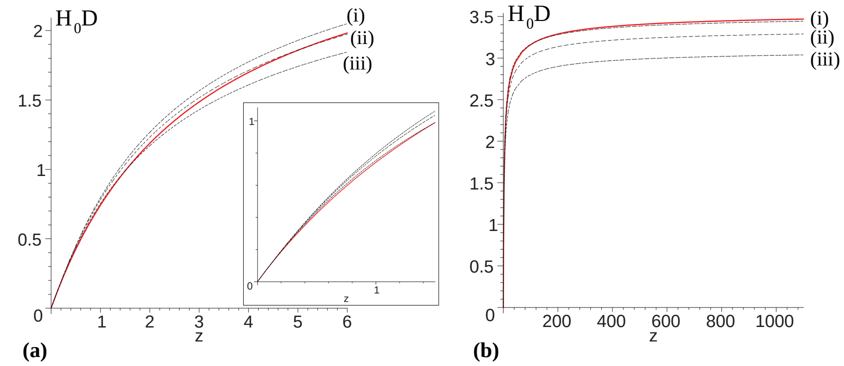

FIGURE 1. The effective comoving distance $H_0D(z)$ is plotted for the best–fit timescape (TS) model, with $f_{v0} = 0.762$, (solid line); and for various spatially flat ΛCDM models (dashed lines). The parameters for the dashed lines are (i) $\Omega_{M0} = 0.249$ (best–fit to WMAP5 only [12]); (ii) $\Omega_{M0} = 0.279$ (joint best–fit to SneIa, BAO and WMAP5); (iii) $\Omega_{M0} = 0.34$ (best–fit to Riess07 SneIa only [13]). Panel (a) shows the redshift range $z < 6$, with an inset for $z < 1.5$, which is the range tested by current SneIa data. Panel (b) shows the range $z < 1100$ up to the surface of last scattering, tested by WMAP5.

does not depend on the value of the Hubble constant, H_0, but only directly on $\Omega_{M0} = 1 - \Omega_{D0}$. Since the best-fit values of H_0 are potentially different for the different scenarios, a comparison of H_0D curves as a function of redshift for the timescape model versus the ΛCDM model gives a good indication of where the largest differences can be expected, independently of the value of H_0. Such a comparison is made in Fig. 1.

We see that as redshift increases the timescape model interpolates between ΛCDM models with different values of Ω_{M0}. For redshifts $z \lesssim 1.5$ $D_{\rm TS}$ is very close to $D_{\Lambda\rm CDM}$ for the parameter values $(\Omega_{M0}, \Omega_{\Lambda0}) = (0.34, 0.66)$ (model (ii)) which best–fit the Riess07 supernovae (SneIa) data [13] only, by our own analysis. For very large redshifts that approach the surface of last scattering, $z \lesssim 1100$, on the other hand, $D_{\rm TS}$ very closely matches $D_{\Lambda\rm CDM}$ for the parameter values $(\Omega_{M0}, \Omega_{\Lambda0}) = (0.249, 0.751)$ (model (i)) which best–fit WMAP5 only [12]. Over redshifts $2 \lesssim z \lesssim 10$, at which scales independent tests are conceivable, $D_{\rm TS}$ makes a transition over corresponding curves of $D_{\Lambda\rm CDM}$ with intermediate values of $(\Omega_{M0}, \Omega_{\Lambda0})$. The $D_{\Lambda\rm CDM}$ curve for joint best fit parameters to SneIa, BAO measurements and WMAP5 [12], $(\Omega_{M0}, \Omega_{\Lambda0}) = (0.279, 0.721)$ is best–matched over the range $5 \lesssim z \lesssim 6$, for example.

The difference of $D_{\rm TS}$ from any single $D_{\Lambda\rm CDM}$ curve are perhaps most pronounced only in the range $2 \lesssim z \lesssim 6$, which may be an optimal regime to probe in future experiments. Gamma–ray bursters (GRBs) now probe distances to redshifts $z \lesssim 8.3$, and could be very useful. There has already been much work deriving Hubble diagrams using GRBs. (See, e.g., [14].) It would appear that more work needs to be done to nail down systematic uncertainties, but GRBs may provide a definitive test in future. An analysis of the timescape model Hubble diagram using 69 GRBs has just been performed by Schaefer [15], who finds that it fits the data better than the concordance ΛCDM model, but not yet by a huge margin. As more data is accumulated, it should become possible to distinguish the models if the issues with the standardization of GRBs can be ironed out.

The effective "equation of state"

It should be noted that the shape of the H_0D curves depicted in Fig. 1 represent the observable quantity one is actually measuring when some researchers loosely talk about "measuring the equation of state". For spatially flat dark energy models, with H_0D given by (9), one finds that the function $w(z)$ appearing in the fluid equation of state $P_D = w(z)\rho_D$ is related to the first and second derivatives of (9) by

$$w(z) = \frac{\frac{2}{3}(1+z)D'^{-1}D'' + 1}{\Omega_{M0}(1+z)^3 H_0^2 D'^2 - 1} \tag{10}$$

where prime denotes a derivative with respect to z. Such a relation can be applied to observed distance measurements, regardless of whether the underlying cosmology has dark energy or not. Since it involves first and second derivatives of the observed quantities, it is actually much more difficult to determine observationally than directly fitting $H_0D(z)$.

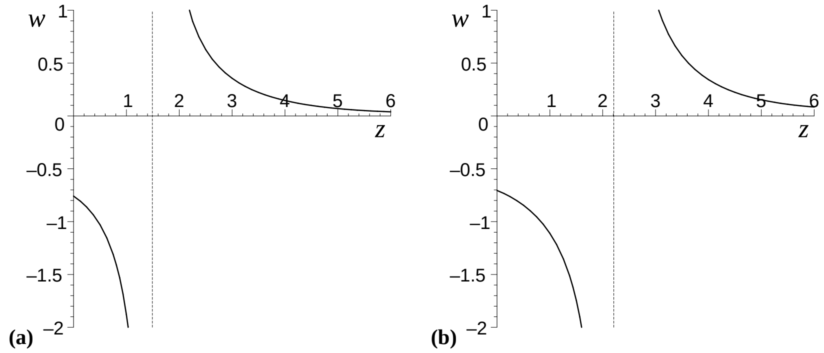

FIGURE 2. The artificial equivalent of an equation of state constructed using the effective comoving distance (10), plotted for the timescape tracker solution with best–fit value $f_{v0} = 0.762$, and two different values of Ω_{M0}: **(a)** the canonical dressed value $\Omega_{M0} = \frac{1}{2}(1 - f_{v0})(2 + f_{v0}) = 0.33$; **(b)** $\Omega_{M0} = 0.279$.

The equivalent of the "equation of state", $w(z)$, for the timescape model is plotted in Fig. 2. The fact that $w(z)$ is undefined at a particular redshift and changes sign through $\pm\infty$ simply reflects the fact that in (10) we are dividing by a quantity which goes to zero for the timescape model, even though the underlying curve of Fig. 1 is smooth. Since one is not dealing with a dark energy fluid in the present case, $w(z)$ simply has no physical meaning. Nonetheless, phenomenologically the results do agree with the usual inferences about w for fits of standard dark energy cosmologies to SneIa data. For the canonical model of Fig. 2(a) one finds that the average value of $w(z) \simeq -1$ on the range $z \lesssim 0.7$, while the average value of $w(z) < -1$ if the range of redshifts is extended to higher values. The fact that $w(z)$ is a different sign to the dark energy case for $z > 2$ is another way of viewing our statement above that the redshift range $2 \lesssim z \lesssim 6$ is optimal for discriminating model differences.

The Alcock–Paczyński test and baryon acoustic oscillations

Alcock and Paczyński devised a test [16] which relies on comparing the radial and transverse proper length scales of spherical standard volumes comoving with the Hubble flow. This test, which determines the function

$$f_{\rm AP} = \frac{1}{z}\left|\frac{\delta\theta}{\delta z}\right| = \frac{HD}{z}, \tag{11}$$

was originally conceived to distinguish FLRW models with a cosmological constant from those without a Λ term. The test is free from many evolutionary effects, but relies on one being able to remove systematic distortions due to peculiar velocities.

Current detections of the BAO scale in galaxy clustering statistics [17, 18] can in fact be viewed as a variant of the Alcock–Paczyński test, as they make use of both the transverse and radial dilations of the fiducial comoving BAO scale to present a measure

$$D_V = \left[\frac{zD^2}{H(z)}\right]^{1/3} = D f_{\rm AP}^{-1/3}. \tag{12}$$

In Fig. 3 the Alcock–Paczyński test function (11) and BAO scale measure (12) of the timescape model are compared to that of spatially flat ΛCDM model with different values of $(\Omega_{\Lambda 0}, \Omega_{\Lambda 0})$. The curve for the timescape model has a distinctly different shape to those of the LCDM models, being convex. However, the extent to which the curves can be reliably distinguished would require detailed analysis based on the precision attainable with any particular experiment. Ideally, a model–independent determination of $H(z)$ would be required since $z f_{\rm AP} = H(z)D(z)$ for all the models under consideration.

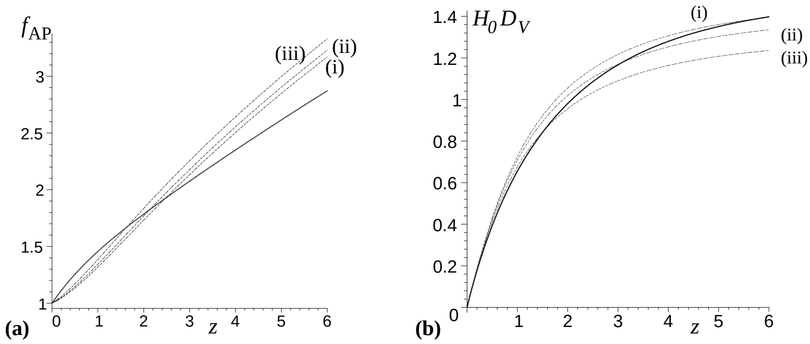

FIGURE 3. **(a)** The Alcock–Paczyński test function $f_{\rm AP} = HD/z$; and **(b)** the BAO radial test function $H_0 D_V = H_0 D f_{\rm AP}^{-1/3}$. In each case the timescape model with $f_{v0} = 0.762$ (solid line) is compared to three spatially flat ΛCDM models with the same values of $(\Omega_{M0}, \Omega_{\Lambda 0})$ as in Fig. 1 (dashed lines).

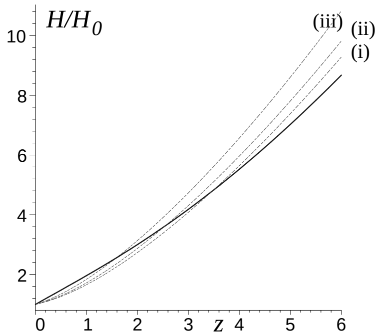

FIGURE 4. The function $H_0^{-1} \frac{\mathrm{d}z}{\mathrm{d}\tau}$ for the timescape model with $f_{v0} = 0.762$ (solid line) is compared to $H_0^{-1} \frac{\mathrm{d}z}{\mathrm{d}t}$ for three spatially flat ΛCDM models with the same values of $(\Omega_{M0}, \Omega_{\Lambda 0})$ as in Fig. 1 (dashed lines).

The $H(z)$ measure

Further observational diagnostics can be devised if the expansion rate $H(z)$ can be observationally determined as a function of redshift. Recently such a determination of $H(z)$ at $z = 0.24$ and $z = 0.43$ has been made using redshift space distortions of the BAO scale in the ΛCDM model [19]. This technique is of course model dependent, and the Kaiser effect would have to be re-examined in the timescape model before a direct comparison of observational results could be made. A model–independent measure of $H(z)$ is discussed in sec. .

In Fig. 4 we compare $H(z)/H_0$ for the timescape model to spatially flat ΛCDM models with the same parameters chosen in Fig. 1. The most notable feature is that the slope of $H(z)/H_0$ is less than in the ΛCDM case, as is to be expected for a model whose (dressed) deceleration parameter varies more slowly than for ΛCDM.

The $Om(z)$ measure

Recently Sahni, Shafieloo and Starobinsky [20] have proposed a new diagnostic of dark energy, the function

$$Om(z) = \left[\frac{H^2(z)}{H_0^2} - 1\right] \left[(1+z)^3 - 1\right]^{-1}, \tag{13}$$

on account of the fact that it is equal to the constant present epoch matter density parameter, Ω_{M0}, for all redshifts for a spatially flat FLRW model with pressureless dust and a cosmological constant, but is not constant if the cosmological constant is replaced by other forms of dark energy. For general FLRW models, $H(z) = [D'(z)]^{-1} \sqrt{1 + \Omega_{k0} H_0^2 D^2(z)}$, which only involves a single derivatives of $D(z)$. Thus the diagnostic (13) is an easier to reconstruct observationally than the equation of state parameter, $w(z)$.

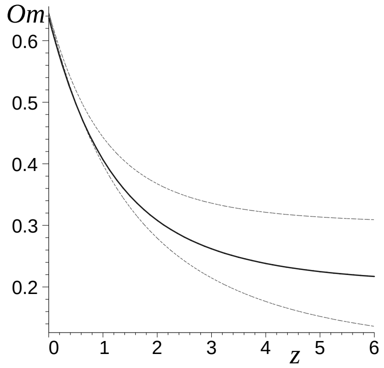

FIGURE 5. The dark energy diagnostic $Om(z)$ of Sahni, Shafieloo and Starobinsky plotted for the timescape tracker solution with best–fit value $f_{v0} = 0.762$ (solid line), and 1σ limits (dashed lines) from ref. [9].

The quantity $Om(z)$ is readily calculated for the timescape model, and the result is displayed in Fig. 5. What is striking about Fig. 5, as compared to the curves for quintessence and phantom dark energy models as plotted in ref. [20], is that the initial value

$$Om(0) = \tfrac{2}{3}\, H'\big|_0 = \frac{2(8f_{v0}^3 - 3f_{v0}^2 + 4)(2 + f_{v0})}{(4f_{v0}^2 + f_{v0} + 4)^2} \tag{14}$$

is substantially larger than in the spatially flat dark energy models. Furthermore, for the timescape model $Om(z)$ does not asymptote to the dressed density parameter Ω_{M0} in any redshift range. For quintessence models $Om(z) > \Omega_{M0}$, while for phantom models $Om(z) < \Omega_{M0}$, and in both cases $Om(z) \to \Omega_{M0}$ as $z \to \infty$. In the timescape model, $Om(z) > \Omega_{M0} \simeq 0.33$ for $z \lesssim 1.7$, while $Om(z) < \Omega_{M0}$ for $z \gtrsim 1.7$. It thus behaves more like a quintessence model for low z, in accordance with Fig. 2. However, the steeper slope and the completely different behaviour at large z mean the diagnostic is generally very different to that of typical dark energy models. For large z, $\bar{\Omega}_{M0} < Om(\infty) < \Omega_{M0}$, if $f_{v0} > 0.25$.

Interestingly enough, a recent analysis of SneIa, BAO and CMB data [21] for dark energy models with two different empirical fitting functions for $w(z)$ gives an intercept $Om(0)$ which is larger than expected for typical quintessence or phantom energy models, and in the better fit of the two models the intercept (see Fig. 3 of ref. [21]) is close to the value $Om(0) = 0.638$ for the $f_{v0} = 0.762$ timescape model.

Test of (in)homogeneity

Recently Clarkson, Bassett and Lu [22] have constructed what they call a "test of the Copernican principle" based on the observation that for homogeneous, isotropic models which obey the Friedmann equation, the present epoch curvature parameter, a constant, may be written as

$$\Omega_{k0} = \frac{[H(z)D'(z)]^2 - 1}{[H_0 D(z)]^2} \tag{15}$$

for all z, irrespective of the dark energy model or any other model parameters. Consequently, taking a further derivative, the quantity

$$\mathscr{C}(z) \equiv 1 + H^2(DD'' - D'^2) + HH'DD' \tag{16}$$

must be zero for all redshifts for any FLRW geometry.

A deviation of $\mathscr{C}(z)$ from zero, or of (15) from a constant value, would therefore mean that the assumption of homogeneity is violated. Although this only constitutes a test of the assumption of the Friedmann equation, i.e., of the Cosmological Principle rather than the broader Copernican Principle adopted in ref. [6], the average inhomogeneity will give a clear and distinct prediction of a non-zero $\mathscr{C}(z)$ for the timescape model.

The functions (15) and (16) are computed in ref. [1]. Observationally it is more feasible to fit (15) which involves one derivative less of redshift. In Fig. 6 we exhibit the function $\mathscr{B}(z) = [HD']^2 - 1$ from the numerator of (15) for

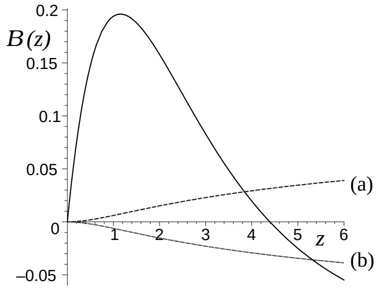

FIGURE 6. The (in)homogeneity test function $\mathscr{B}(z) = [HD']^2 - 1$ is plotted for the timescape tracker solution with best–fit value $f_{v0} = 0.762$ (solid line), and compared to the equivalent curves $\mathscr{B} = \Omega_{k0}(H_0 D)^2$ for two different ΛCDM models with small curvature: **(a)** $\Omega_{M0} = 0.28$, $\Omega_{\Lambda 0} = 0.71$, $\Omega_{k0} = 0.01$; **(b)** $\Omega_{M0} = 0.28$, $\Omega_{\Lambda 0} = 0.73$, $\Omega_{k0} = -0.01$. A spatially flat FLRW model would have $\mathscr{B}(z) \equiv 0$.

the timescape model, as compared to two ΛCDM models with a small amount of spatial curvature. In the FLRW case $\mathscr{B}(z)$ is always a monotonic function whose sign is determined by that of Ω_{k0}. An open $\Lambda = 0$ universe with the same Ω_{M0} would have a monotonic function $\mathscr{B}(z)$ very much greater than that of the timescape model.

Time drift of cosmological redshifts

For the purpose of the $Om(z)$ and (in)homogeneity tests considered in the last section, $H(z)$ must be observationally determined, and this is difficult to achieve in a model independent way. There is one way of achieving this, however, namely by measuring the time variation of the redshifts of different sources over a sufficiently long time interval [23], as has been discussed recently by Uzan, Clarkson and Ellis [24]. Although the measurement is extremely challenging, it may be feasible over a 20 year period by precision measurements of the Lyman-α forest in the redshift range $2 < z < 5$ with the next generation of Extremely Large Telescopes [25].

In ref. [1] an analytic expression for $H_0^{-1}\frac{\mathrm{d}z}{\mathrm{d}\tau}$ is determined, the derivative being with respect to wall time for observers in galaxies. The resulting function is displayed in Fig. 4 for the best-fit timescape model with $f_{v0} = 0.762$, where it is compared to the equivalent function for three different spatially flat ΛCDM models. What is notable is that the curve for the timescape model is considerably flatter than those of the ΛCDM models. This may be understood to arise from the fact that the magnitude of the apparent acceleration is considerably smaller in the timescape model, as compared to the magnitude of the acceleration in ΛCDM models. For models in which there is no apparent acceleration whatsoever, one finds that $H_0^{-1}\frac{\mathrm{d}z}{\mathrm{d}\tau}$ is always negative. If there is cosmic acceleration, real or apparent, at late epochs then $H_0^{-1}\frac{\mathrm{d}z}{\mathrm{d}\tau}$ will become positive at low redshifts, though at a somewhat larger redshift than that at which acceleration is deemed to have begun.

Fig. 4 demonstrates that a very clear signal of differences in the redshift time drift between the timescape model and ΛCDM models might be determined at low redshifts when $H_0^{-1}\frac{\mathrm{d}z}{\mathrm{d}\tau}$ should be positive. In particular, the magnitude of $H_0^{-1}\frac{\mathrm{d}z}{\mathrm{d}\tau}$ is considerably smaller for the timescape model as compared to ΛCDM models. Observationally, however, it is expected that measurements will be best determined for sources in the Lyman α forest in the range, $2 < z < 5$. At such redshifts the magnitude of the drift is somewhat more pronounced in the case of the ΛCDM models. For a source at $z = 4$, over a period of $\delta\tau = 10$ years we would have $\delta z = -3.3 \times 10^{-10}$ for the timescape model with $f_{v0} = 0.762$ and $H_0 = 61.7\,\mathrm{km\ sec^{-1}\,Mpc^{-1}}$. By comparison, for a spatially flat ΛCDM model with $H_0 = 70.5\,\mathrm{km\ sec^{-1}\,Mpc^{-1}}$ a source at $z = 4$ would over ten years give $\delta z = -4.7 \times 10^{-10}$ for $(\Omega_{M0}, \Omega_{\Lambda 0}) = (0.249, 0.751)$, and $\delta z = -7.0 \times 10^{-10}$ for $(\Omega_{M0}, \Omega_{\Lambda 0}) = (0.279, 0.721)$.

DISCUSSION

The tests outlined here demonstrate several lines of investigation to distinguish the timescape model from models of homogeneous dark energy. The (in)homogeneity test of Bassett, Clarkson and Lu is definitive, since it tests the validity of the Friedmann equation directly.

In performing these tests, however, one must be very careful to ensure that data has not been reduced with built–in assumptions that use the Friedmann equation. For example, current estimates of the BAO scale such as that of Percival *et al*. [18] do not determine D_V directly from redshift and angular diameter measures, but first perform a Fourier space transformation to a power spectrum, assuming an FLRW cosmology.

Furthermore, in the case of SneIa, it has been recently claimed [26] that the timescape model does not compare favourably with the ΛCDM model when SneIa from the recent Union [27] and Constitution [28] compilations are used. However, the Union dataset and its extension use the SALT method to calibrate light curves. In this approach empirical light curve parameters and cosmological parameters – *assuming the Friedmann equation* – are simultaneously fit by analytic marginalisation before the raw apparent magnitudes are recalibrated. As Hicken *et al*. discuss [28], a number of possible systematic discrepancies exist between data reduced by the SALT, SALT2, MLCS31 and MLCS17 techniques. In the case of the timescape model, for which the Friedmann equation does not apply, it turns out that these systematic differences lead to larger discrepancies in the determination of cosmological parameters from one method to another, as will be discussed in future work [29].

The value of the dressed Hubble constant is also an observable quantity of considerable interest. A recent determination by Riess *et al*. [30] poses a challenge for the timescape model. However, in the presence of spatial curvature gradients a great deal of care must be taken, since in view of the expected Hubble bubble feature discussed in Sec. , estimates of H_0 made below the scale of statistical homogeneity will generally give higher values. The method that is used to anchor the Cepheid calibration in the SH_0ES survey [30] – namely a geometric maser distance to the relatively close galaxy NGC4258 – may in fact be the best way of determining whether a Hubble bubble feature exists, if sufficiently large numbers of maser distances can be determined within the scale of statistical homogeneity. The Megamaser project [31] may soon begin to provide the sort of data that is required.

ACKNOWLEDGMENTS

I thank Prof. Remo Ruffini and ICRANet for support and hospitality while the work of ref. [1] was undertaken. This work was also partly supported by the Marsden fund of the Royal Society of New Zealand.

REFERENCES

1. D.L. Wiltshire, Phys. Rev. **D**, in press; arXiv:0909.0749.
2. D.L. Wiltshire, in *Dark Matter in Astroparticle and Particle Physics: Proceedings of the 6th International Heidelberg Conference*, eds H.V. Klapdor–Kleingrothaus and G.F. Lewis, (World Scientific, Singapore, 2008) pp. 565-596 [arXiv:0712.3984].
3. F. Hoyle and M.S. Vogeley, ApJ **566**, 641 (2002); ApJ **607**, 751 (2004).
4. T. Buchert, Gen. Relativ. Grav. **32**, 105 (2000); Gen. Relativ. Grav. **33**, 1381 (2001).
5. T. Buchert, Gen. Relativ. Grav. **40**, 467 (2008).
6. D.L. Wiltshire, New J. Phys. **9**, 377 (2007).
7. D.L. Wiltshire, Phys. Rev. Lett. **99**, 251101 (2007).
8. D.L. Wiltshire, Phys. Rev. **D 78**, 084032 (2008).
9. B.M. Leith, S.C.C. Ng and D.L. Wiltshire, ApJ **672**, L91 (2008).
10. S. Jha, A.G. Riess and R.P. Kirshner, ApJ **659**, 122 (2007).
11. N. Li and D.J. Schwarz, Phys. Rev. **D78**, 083531 (2008).
12. E. Komatsu *et al*., Astrophys. J. Suppl. **180**, 330 (2009).
13. A.G. Riess *et al*., ApJ **659**, 98 (2007).
14. B.E. Schaefer, ApJ **660**, 16 (2007); N. Liang, W. K. Xiao, Y. Liu and S.N. Zhang, ApJ **685**, 354 (2008). L. Amati, C. Guidorzi, F. Frontera, M. Della Valle, F. Finelli, R. Landi and E. Montanari, MNRAS **391**, 577 (2008); R. Tsutsui, T. Nakamura, D. Yonetoku, T. Murakami, Y. Kodama and K. Takahashi, arXiv:0810.1870.
15. B.E. Schaefer, in preparation.
16. C. Alcock and B. Paczyński, Nature **281**, 358 (1979).
17. D.J. Eisenstein *et al*., ApJ **633** (2005) 560; S. Cole *et al*., MNRAS **362** (2005) 505.
18. W.J. Percival *et al*., MNRAS **381**, 1053 (2007).
19. E. Gaztañaga, A. Cabre and L. Hui, arXiv:0807.3551.
20. V. Sahni, A. Shafieloo and A. A. Starobinsky, Phys. Rev. **D 78**, 103502 (2008).
21. A. Shafieloo, V. Sahni and A.A. Starobinsky, arXiv:0903.5141.
22. C. Clarkson, B. Bassett and T.C. Lu, Phys. Rev. Lett. **101**, 011301 (2008).

23. A. Sandage, ApJ **136**, 319 (1962); G.C. McVittie, ApJ **136**, 334 (1962); A. Loeb, ApJ **499**, L111 (1998).
24. J.P. Uzan, C. Clarkson and G.F.R. Ellis, Phys. Rev. Lett. **100**, 191303 (2008).
25. P.S. Corasaniti, D. Huterer and A. Melchiorri, Phys. Rev. **D75**, 062001 (2007); J. Liske *et al.*, MNRAS **386**, 1192 (2008).
26. J. Kwan, M.J. Francis and G.F. Lewis, arXiv:0902.4249.
27. M. Kowalski *et al*., ApJ **686**, 749 (2008).
28. M. Hicken *et al*., arXiv:0901.4804.
29. P.R. Smale and D.L. Wiltshire, in preparation.
30. A.G. Riess *et al*., ApJ **699**, 539 (2009).
31. M.J. Reid, J.A. Braatz, J.J. Condon, L. . Greenhill, C. Henkel and K.Y. Lo, ApJ **695**, 287 (2009).